Evaluation and Optimization of High Collapse Resistance Casing Strings for Salt Cavern Gas Storage in Salt Formations

Guanghai Zhu[1], Wenquan Wang[1], Haoyu Diao[2,*], Fansheng Ban[2], Haotian Xiong[1], Xingwei Hou[1], Xiaoxu Liu[1] and Tao Ma[1]

[1] PipeChina Engineering Technology Innovation Co., Ltd., Tianjin, 300450, China

[2] CNPC Engineering Technology R&D Company Limited, Beijing, 102206, China

Evaluation and Optimization of High Collapse Resistance Casing Strings for Salt Cavern Gas Storage in Salt Formations

Guanghai Zhu[1]**, Wenquan Wang**[1]**, Haoyu Diao**[2,*]**, Fansheng Ban**[2]**, Haotian Xiong**[1]**, Xingwei Hou**[1]**, Xiaoxu Liu**[1] **and Tao Ma**[1]

[1] PipeChina Engineering Technology Innovation Co., Ltd., Tianjin, 300450, China

[2] CNPC Engineering Technology R&D Company Limited, Beijing, 102206, China

ABSTRACT

Salt cavern gas storage imposes stringent requirements on casing performance due to salt rock creep and high *in-situ* stress, necessitating a balance between mechanical strength and economic viability. This study evaluates the collapse resistance of BG110V and BG140V casings under 50°C–85°C through full-scale experiments (ASTM E2948) and elastoplastic finite element simulations. Results show that BG140V achieves a collapse strength of 75.94 MPa at 85°C, surpassing BG110V (52.96 MPa) at the same temperature by 43.4%, attributed to its thick-walled design (17.50 mm vs. BG110V's 15.88 mm) and material enhancements. Simulations reveal lower prediction errors for BG140V (5.9% in full collapse) compared to BG110V (20.6%). A multi-criteria model integrating collapse strength (0.5), temperature sensitivity (0.3), and life-cycle cost (LCC, 0.2) with Monte Carlo analysis demonstrates BG140V's LCC advantage in deep reservoirs (creep rate $> 1.2 \times 10^{-7}$ s^{-1}, 12% maintenance cost reduction), while BG110V suits shallow scenarios (18% lower procurement cost). Dynamic selection strategies with real-time monitoring, low-friction thread optimization, crystal plasticity simulations, and smart maintenance systems are proposed. This study provides a quantitative framework for balancing safety and economy, advancing the standardization of non-API casings.

1 Introduction

Salt cavern gas storage has become a core facility for global strategic energy reserves due to its high safety and peak-shaving capabilities [1,2]. Relevant studies have further confirmed its engineering value in energy storage applications [3–5]. However, the creep effect of salt rock formations under long-term high-pressure injection-production cycles can easily lead to external collapse instability of the casing, seriously threatening the integrity of the storage facility [6]. Subsequent research has supplemented the mechanisms of casing failure induced by salt rock creep [7]. Statistics indicate that approximately

---

1

G. Zhu, W. Wang, H. Diao, F. Ban, H. Xiong, X. Hou, X. Liu and Tao Ma,
Evaluation and optimization of high collapse resistance casing strings
for salt cavern gas storage in salt formations,
Rev. int. métodos numér. cálc. diseño ing. (2026). Vol.42, (1), 9

12% of salt cavern gas storage accidents worldwide are directly related to casing collapse [8], making the optimization of casing selection an urgent engineering challenge.

Current research on casing collapse resistance primarily focuses on material improvement and structural optimization. For example, Sarmad Khubaib et al. [9] enhanced the low-temperature impact toughness of medium-carbon oil casing steel by controlling tundish superheat, calcium-sulfur mass ratio, and rolling deformation, revealing the influence mechanism of microstructural control on material resistance to brittle fracture. However, this study did not address the high-temperature stability requirements in salt rock creep environments. Relevant studies established a safety factor calculation model and optimized specifications for scenarios with cement sheath absence, demonstrating the critical importance of the synergistic effect between casing-cement sheath-formation on load-bearing capacity [10–13]. However, existing research has not systematically quantified the impact of non-uniform loads caused by salt rock creep on this synergistic system [14].

Regarding multi-physical field coupling mechanisms, scholars have gradually focused on the attenuation effect of temperature-stress-fluid coupling on casing performance. Existing research mainly focuses on hydraulic fracturing scenarios and lacks real-time coupling analysis of salt rock creep-casing deformation, especially the validation of scale effects between small-scale specimens and engineering prototypes in full-size models [10]. Xi et al. [15] revealed the degradation pattern of cement sheath integrity during multi-stage hydraulic fracturing in shale gas wells through numerical simulation, finding that high-temperature, high-pressure fluid penetration intensifies interfacial failure between the casing and cement sheath. Shen et al. [16] simulated deformation and stress characteristics of casing in tight oil fracturing based on elastoplastic finite element analysis, confirming that the equivalent plastic strain of the casing increases by 15%–20% for every 10°C increase in temperature gradient. Further gaps exist in the scale effects of full-size models [17–19]. Although Lian et al. [20] proposed a geomechanical model for casing deformation in shale gas horizontal wells, it did not cover the load evolution laws specific to the steady-state and accelerated creep stages of salt rock.

The application of numerical simulation technology has promoted the refinement of casing performance prediction. However, existing simulations mostly rely on homogeneous material assumptions, neglecting salt rock anisotropic creep (such as the bedding dependence of Norton-Bailey model parameters) and simplifying the friction effects at casing threaded connections [21,22]. Sun et al. [23] introduced a random forest algorithm to establish a casing deformation prediction model, improving prediction accuracy by 22% compared to traditional finite element methods in multi-factor coupling scenarios. Tian et al. [24] simulated the repair force for high-grade casing using a segmented reamer and proposed a shaping load calculation method based on energy conservation. Additionally, Fu et al. [25] proposed an analytical calculation method for the pass-through capability of deformed casing, but it did not address the dynamic influence of material softening on cross-sectional deformation under high temperatures.

In terms of economic analysis, it had proposed a casing selection framework based on Life Cycle Cost (LCC), but failed to establish a quantitative relationship between strength degradation and maintenance costs [26–29]. In existing research, Cao et al. [30], through economic sensitivity analysis of cementing quality and casing failure, pointed out that shallow storage facilities using low-cost casing need to reserve a 20% maintenance cost buffer. However, the long-term economic benefits of material upgrades in deep high-temperature scenarios still lack support from multi-objective optimization models.

In summary, existing research often focuses on single factors (such as mechanical performance or economics), lacking a systematic multi-dimensional analysis of strength, temperature sensitivity,

G. Zhu, W. Wang, H. Diao, F. Ban, H. Xiong, X. Hou, X. Liu and Tao Ma,
Evaluation and optimization of high collapse resistance casing strings
for salt cavern gas storage in salt formations,
Rev. int. métodos numér. cálc. diseño ing. (2026). Vol.42, (1), 9

and cost. Significant gaps also exist in the dynamic characterization of salt rock creep loads, the collapse characteristics of full-size casings, and real-time decision-making mechanisms for engineering selection. This paper takes BG110V and BG140V casings as research objects. Through full-scale collapse experiments (ASTM E2948 standard) and elastoplastic finite element simulation (Abaqus Explicit), it systematically quantifies the influence of temperature (50°C–85°C) on collapse resistance. Combined with an LCC model, a dynamic selection method based on creep rate is proposed. The innovations are: (1) Establishing for the first time a full-scale experimental system considering salt rock creep-casing deformation coupling, bridging the scale difference between small specimens and engineering prototypes; (2) Proposing a multi-objective optimization model based on strength attenuation rate and cost sensitivity coefficient, providing a quantitative basis for casing selection in deep salt cavern gas storage.

2 Experimental Setup and Methodology

2.1 Text Layout

Geometric Dimension Measurement: Before testing, geometric dimensions such as outer diameter (OD), wall thickness (WT), OD ovality, and WT eccentricity of the casing specimens were measured. Starting from one end of the casing body, a grid was divided every 345 mm, resulting in 8 measurement cross-sections. On each cross-section, measurement points were spaced every 45°, totaling 8 points per section. After testing, the OD of the failed casing specimen was measured using the same method (Fig. 1).
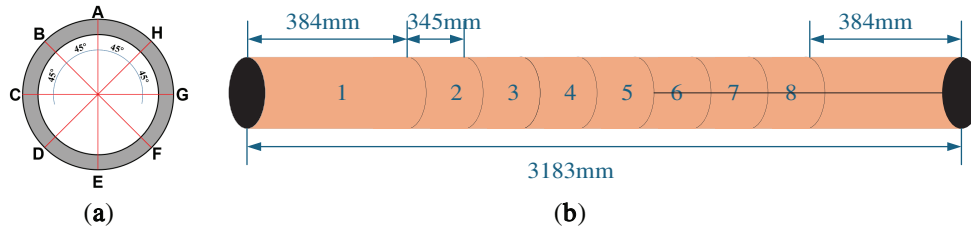

Figure 1: (a) Cross-sectional distribution of sample pipes, **(b)** Geometric shape test diagram

Residual Stress Test: Residual stress testing was performed. Before the test, 5 cross-sections of the specimen were measured, with 8 measurement points per section spaced every 45°. After the residual stress test, the OD values of the same 5 cross-sections were measured again. Residual stress was calculated using the following Formula (1):

$$\sigma_{res} = Et_{ave}\left(\frac{1}{D_{ac}} - \frac{1}{D_{bc}}\right)/\left(1 - v^2\right) \tag{1}$$

where: σ_{res}—Residual stress; E—Elastic modulus (206.9 GPa); t_{ave}—Average wall thickness; D_{ac}—OD before test; D_{bc}—OD after test; v—Poisson's ratio (0.28).

External Pressure Collapse Test: According to ISO 13679:2002(E) standard, external pressure to failure tests were conducted on $\Phi339.7 \times 15.88$ mm BG110V casing and $\Phi339.7 \times 17.50$ mm BG140V casing at 50°C and 85°C. The tests were performed on the Collapse & Burst Tester (Serial No.: MRIE-Z3940) at Xi'an Moore Petroleum Engineering Laboratory Co., Ltd. This equipment consists of a triaxial loading system (axial pressure 0–150 MPa, radial pressure 0–100 MPa), a temperature control module (20°C–120°C, accuracy ±1.5°C), and a data acquisition unit (sampling frequency 1 kHz). To

G. Zhu, W. Wang, H. Diao, F. Ban, H. Xiong, X. Hou, X. Liu and Tao Ma,
Evaluation and optimization of high collapse resistance casing strings
for salt cavern gas storage in salt formations,
Rev. int. métodos numér. cálc. diseño ing. (2026). Vol.42, (1), 9

simulate the salt rock creep process, radial pressure was applied via an electro-hydraulic servo closed-loop control system at a loading rate of 0.05 MPa/s (as required by ASTME2948 ≤0.1 MPa/s). Casing samples had a length-to-outer diameter ratio of 5:1 (1698.5 mm), meeting ASTM E2948's requirement for full-scale experiments (≥4:1). Deionized water (resistivity ≥ 18 MΩ·cm) was used as the pressure medium. A constant-temperature circulation system maintained stability within ±1.5°C.

Strain Measurement: Surface strain fields of the casing were measured using high-precision resistance strain gauges (HBM LY71-6/120, temperature compensation range—30°C to 150°C). Strain gauges were arranged circumferentially (0°, 90°, 180°, 270°) and axially at equal intervals, with 5 axial stations spaced 100 mm apart. They were bonded to the casing surface using epoxy resin adhesive (Loctite EA 9396), ensuring strain transfer efficiency ≥95%. After attaching the strain gauges, the sample was installed in the external pressure chamber, and the strain gauge leads were connected and tested with the strain acquisition instrument. During the pressurization of the external pressure, the strain changes on the casing surface were collected in real time until the casing failed (Fig. 2).

Figure 2: Field physical diagram

3D Dimensional Model Scanning: After testing, the failed casing specimen was scanned using a 3D scanner to establish a high-precision model and measure the dimensions and shape changes of the failed casing. This provides an intuitive understanding of the deformation during the test and offers more accurate data for numerical simulation.

The main experimental process is shown in Fig. 3 below:

2.2 Main Experimental Results

Collapse results are shown in Tables 1 and 2 below:

Comparison of Geometric Deformation between Initial State and after Collapse: The OD, WT, and other geometric parameters of the casing in the initial state and after collapse were measured, comparing geometric deformation under different temperatures. See Tables 3 and 4 below.
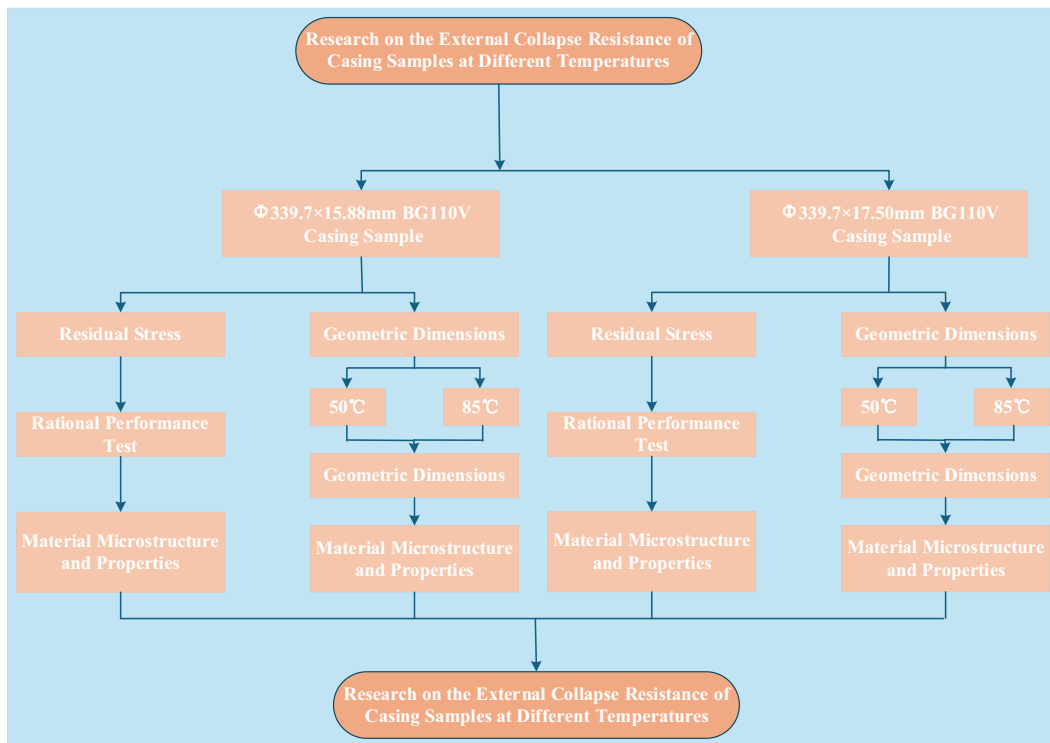
G. Zhu, W. Wang, H. Diao, F. Ban, H. Xiong, X. Hou, X. Liu and Tao Ma,
Evaluation and optimization of high collapse resistance casing strings
for salt cavern gas storage in salt formations,
Rev. int. métodos numér. cálc. diseño ing. (2026). Vol.42, (1), 9

Figure 3: Flow chart of external pressure collapse test for casing physical samples (based on ASTM E2948 standard)

Table 1: Test results of external pressure to failure for Φ339.7 × 15.88 mm BG110V casing under high-temperature conditions

Test temp.	Pressure medium	Result	
		Collapse pressure (MPa)	Failure mode
50°C	Water	56.72	Collapse at mid-body
85°C	Water	52.96	Collapse at mid-body

Table 2: Test results of external pressure to failure for Φ339.7 × 17.50 mm BG140V casing under high-temperature conditions

Test temp.	Pressure medium	Result	
		Collapse pressure (MPa)	Failure mode
50°C	Water	83.42	Collapse at mid-body
85°C	Water	75.94	Collapse at mid-body

G. Zhu, W. Wang, H. Diao, F. Ban, H. Xiong, X. Hou, X. Liu and Tao Ma,
Evaluation and optimization of high collapse resistance casing strings
for salt cavern gas storage in salt formations,
Rev. int. métodos numér. cálc. diseño ing. (2026). Vol.42, (1), 9

Table 3: Geometric dimension measurement results (mm) of $\Phi339.7 \times 15.88$ mm BG110V casing after test

Section		A–E (mm)	B–F (mm)	C–G (mm)	D–H (mm)	Avg. (mm)	Ovality (%)
1	OD	341.04	341.47	341.53	341.33	341.32	0.19
2	OD	341.06	341.25	341.92	341.51	341.47	0.25
3	OD	341.35	341.25	341.14	341.09	341.21	0.07
4	OD	341.57	341.66	340.96	341.87	341.53	0.24
5	OD	341.18	341.09	341.05	341.36	341.16	0.10
6	OD	342.64	342.53	342.34	342.25	342.44	0.14
7	OD	342.13	342.16	342.29	342.34	342.23	0.06
8	OD	341.66	341.47	341.33	341.55	341.52	0.08

Table 4: Geometric dimension measurement results (mm) of $\Phi339.7 \times 17.50$ mm BG140V casing after test

Section		A–E (mm)	B–F (mm)	C–G (mm)	D–H (mm)	Avg. (mm)	Ovality (%)
1	OD	341.14	341.63	343.41	342.25	342.13	0.69
2	OD	330.04	343.85	352.22	343.54	342.46	6.58
3	OD	307.28	337.77	373.69	345.78	341.13	19.64
4	OD	278.54	333.03	387.04	338.06	334.16	31.98
5	OD	287.54	333.02	387.01	338.05	336.41	29.47
6	OD	317.65	336.34	364.93	335.59	338.68	13.82
7	OD	335.83	340.13	347.69	341.02	341.19	3.49
8	OD	342.81	341.82	341.24	342.01	342.02	0.45

Note: 1. A-E, B-F, C-G, D-H refer to diameter measurements at 0°–180°, 45°–225°, 90°–270°, and 135°–315° angular positions, respectively. 2. Extreme deformation in localized sections may reduce the representativeness of the average OD. Ovality calculated as: [(max OD − min OD)/avg OD] × 100%.

For different casing types, the effect of temperature on collapse pressure shows significant differences. For the $\Phi339.7 \times 15.88$ mm BG110V casing, when the temperature increased from 50°C to 85°C, the collapse pressure decreased from 56.72 to 52.96 MPa. This phenomenon may be attributed to microstructural changes in the material at higher temperatures, inducing some strengthening effect. In contrast, for the $\Phi339.7 \times 17.50$ mm BG140V casing, within the same temperature range, the collapse pressure *decreased*. It is speculated that the reason may be that the material softening effect caused by high temperature outweighed other potential strengthening factors. Furthermore, comparing the experimental results with existing theoretical models helps to deeply explore the causes of differences and guide subsequent research on casing performance.

In contrast, the deformation of the $\Phi339.7 \times 17.50$ mm BG140V casing is more complex, with large variations in ovality. An in-depth analysis of the reasons indicates that temperature affects the coefficient of thermal expansion and mechanical properties of the material, and the characteristics of the pressure medium, as well as the size and wall thickness of the casing, may all play a role. Overall, different performance optimization directions should be proposed for different casing types. For

G. Zhu, W. Wang, H. Diao, F. Ban, H. Xiong, X. Hou, X. Liu and Tao Ma,
Evaluation and optimization of high collapse resistance casing strings
for salt cavern gas storage in salt formations,
Rev. int. métodos numér. cálc. diseño ing. (2026). Vol.42, (1), 9

instance, for BG110V casing, further exploration on utilizing the limited strengthening effect brought by temperature increase is needed; For the 0339.7 × 15.88 mm BG110V casing, when the temperature increased from 50°C to 85°C, the collapse pressure decreased from 56.72 to 52.96 MPa. This anomaly contradicts conventional thermal softening theory. Further analysis of tensile data (Table 5) reveals a 4.4% reduction in yield strength (917.4→879.0 MPa) and 17.8% loss of uniform elongation (Fig. 4), indicating accelerated plastic instability under combined thermal-creep loading.

Table 5: Tensile test results of Φ339.7 × 15.88 mm BG110V casing body material

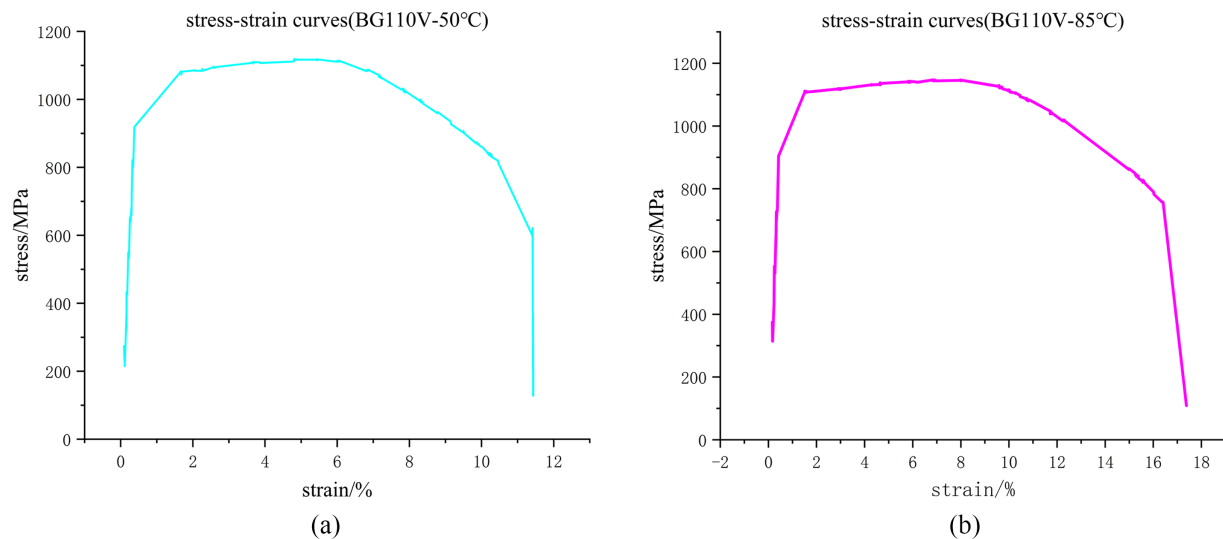| Test temp. (°C)	Test type	Sampling direction	Yield strength Rt0.5 (MPa)	Tensile strength Rm (MPa)	Elongation after fracture (%)
50	Tension	Longitudinal	917.4	1026.8	21.12
85	Tension	Longitudinal	879.0	997.9	17.82

Figure 4: Stress-strain curves of BG110V (**a**): 50°C, (**b**): 85°C

2.3 Stress-Strain Analysis of Tensile Tests for Different Sampled Materials

Tensile tests were conducted on different sampled materials, recording stress-strain curves. The stress-strain curve (Each curve is the average of 3 repeated tests, with a coefficient of variation <3%) relationships were regressed as shown in Figs. 4 and 5. See Tables 5 and 6:

From the tables, it can be seen that the mechanical properties of materials vary depending on the sampling direction. The yield strength and tensile strength of longitudinally sampled materials are generally higher than transversely sampled ones, while the elongation after fracture is relatively lower. This is because the microstructure and mechanical properties of the material vary in different directions, which needs to be considered in the design and use of casings regarding the influence of sampling direction on material performance.
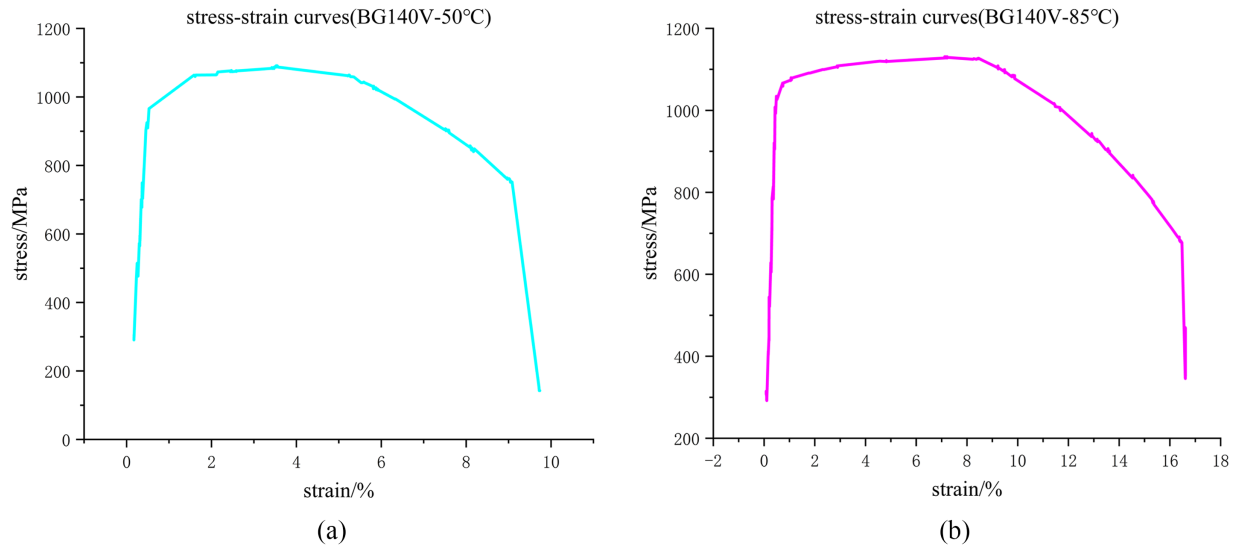
G. Zhu, W. Wang, H. Diao, F. Ban, H. Xiong, X. Hou, X. Liu and Tao Ma,
Evaluation and optimization of high collapse resistance casing strings
for salt cavern gas storage in salt formations,
Rev. int. métodos numér. cálc. diseño ing. (2026). Vol.42, (1), 9

Figure 5: Stress-strain curves of BG140V (**a**): 50°C, (**b**): 85°C

Table 6: Tensile test results of Φ339.7 × 17.50 mm BG140V casing body material

Test temp. (°C)	Test type	Sampling direction	Yield strength Rt0.5 (MPa)	Tensile strength Rm (MPa)	Elongation after fracture (%)
50	Tension	Longitudinal	1074.4	1143.6	19.67
85	Tension	Longitudinal	1037.6	1116.0	17.91

Note: 1. $R_{t0.5}$ refers to yield strength at 0.5% plastic strain. 2. Transverse sampling data are available in the supplementary materials.

3 Numerical Simulation of External Pressure Collapse for Non-Standard High Toughness Casing

3.1 Main Numerical Simulation Process and Model

Based on the Abaqus/Explicit platform, a 3D elastoplastic model of the casing-salt rock system was constructed (Fig. 6). The casing was discretized using C3D8R reduced integration elements, with element size determined as 5 mm through sensitivity analysis (encrypted to 2 mm in edge regions), edge regions refer to threaded connections and stress concentration zones. The salt rock domain employed a Drucker-Prager model coupled with the Norton-Bailey creep constitutive equation (Eq. (2)) to capture both plastic yielding and time-dependent deformation, with parameters calibrated through uniaxial creep tests (Table 7). The casing-salt rock interface was defined with frictional contact (friction coefficient 0.15, normal hard contact). Boundary conditions simulated actual working conditions: the salt rock bottom surface was fixed (U1 = U2 = U3 = 0), the top surface was subjected to equivalent overburden pressure (20 MPa); the casing inner and outer walls were subjected to drilling fluid pressure (P_{in} = 15 MPa) and salt rock creep external pressure ($P_{ext(t)}$ time-varying loading), respectively.
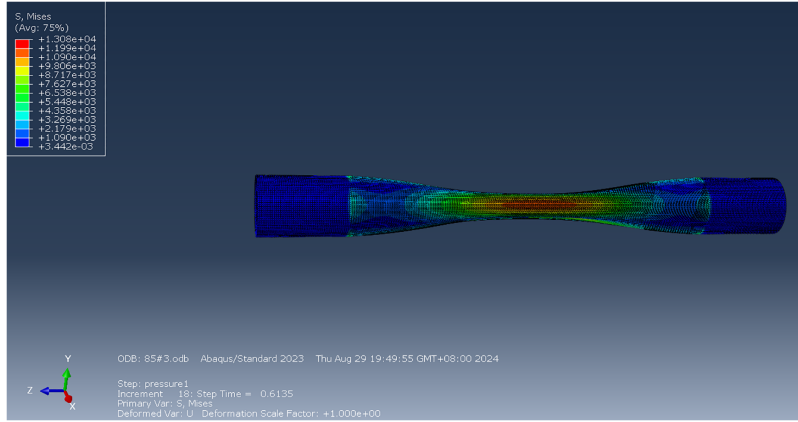
Figure 6: Simulation animation of casing

Table 7: Collapse pressure sensitivity to friction coefficient (Units: MPa)

Friction coefficient (μ)	BG110V at 50°C	BG110V at 85°C	BG140V at 50°C	BG140V at 85°C
0.05	58.2	54.5	85.1	80.1
0.10	57.3	53.6	84.0	78.3
0.15	56.7	52.9	83.4	75.9
0.20	55.8	51.8	82.3	72.6
0.25	54.6	50.5	81.0	70.8

Constitutive Equations:

Salt Rock Creep Strain Rate (Norton-Bailey model):

$$\dot{\varepsilon}_c = A \cdot \sigma_{eff}{}^n \cdot e^{-Q/(RT)} \tag{2}$$

where: $A = 3.2 \times 10^{-8}$ MPa^{-n}/s,

$n = 3.1$, $Q = 65$ kJ/mol,

$R = 8.314$ J (mol/cdotpK).

Casing Elastoplastic Model (J2 flow rule)

$$\sigma_y = \sigma_0 + K \cdot \varepsilon_p{}^m \tag{3}$$

where:

BG110V: $\sigma_0 = 758$ MPa, $K = 1020$ MPa, $m = 0.12$;

BG140V: $\sigma_0 = 965$ MPa, $K = 1250$ MPa, $m = 0.09$.

where: m is the strain hardening exponent, derived from uniaxial tensile tests

A comprehensive parametric study was added to quantify the impact of casing-salt rock interface friction on collapse pressure. The analysis covers both BG110V and BG140V casings at 50°C and 85°C, with friction coefficients (μ) ranging from 0.05 to 0.25. Key findings (Table 7):

Friction coefficient variation alters collapse pressure by up to 11.7%, validating the need for low-friction thread optimization ($\mu < 0.1$) proposed in Section 4.2.

G. Zhu, W. Wang, H. Diao, F. Ban, H. Xiong, X. Hou, X. Liu and Tao Ma,
Evaluation and optimization of high collapse resistance casing strings
for salt cavern gas storage in salt formations,
Rev. int. métodos numér. cálc. diseño ing. (2026). Vol.42, (1), 9

BG140V exhibits greater sensitivity: Higher μ reduces collapse pressure more severely due to its thick-walled design (17.50 mm), amplifying stress concentrations.

For BG110V, μ increases from 0.05 to 0.25 reduce collapse pressure by 6.2% (50°C) and 7.3% (85°C), highlighting vulnerability in thin-walled designs.

For BG140V, reductions reach 5.1% (50°C) and 11.7% (85°C), underscoring temperature-friction synergy. This data justifies low-friction thread development in Section 4.2.

3.2 Main Simulation Results

Analysis of experimental data shows that the experimental collapse strengths of BG110V casing at 50°C and 85°C were 56.72 and 52.96 MPa, respectively, both lower than the deformation initiation pressure (59.65 and 55.43 MPa) and full collapse pressure (71.45 and 67.45 MPa) of its simulation model. This suggests that the simulation model may overestimate material uniformity and the influence of high-temperature softening effects. In contrast, the BG140V casing exhibited significantly higher experimental values (83.42 and 75.94 MPa) than BG110V under the same temperatures, with smaller error ranges compared to simulation results (10.5% error(error = |(Simulated Value-Experimental Value)/Experimental Value| × 100%) in deformation initiation pressure at 50°C, 5.9% error in full collapse). This validates the stability advantage of its thick-walled design (17.50 mm) and strengthened material under high-temperature creep conditions. However, note that minor deviations between the simulation's full collapse stage (e.g., 83.33 MPa at 85°C) and experimental values might stem from simplified assumptions regarding the interface friction coefficient; it is recommended to optimize model parameters by incorporating microstructural analysis. The simulation animation is shown in Fig. 6, and simulation results are summarized in Table 8.

Table 8: Simulation results of BG110V and BG140V casings

Casing model	Temp.	Test result (MPa)	Simulated deformation initiation pressure (MPa)	Simulated full collapse pressure (MPa)
Φ339.7 mm × 15.88 mm BG110V	50°C	56.72	59.65	71.45
Φ339.7 mm × 15.88 mm BG110V	85°C	52.96	55.43	67.45
Φ339.7 mm × 17.50 mm BG140V	50°C	83.42	75.46	88.72
Φ339.7 mm × 17.50 mm BG140V	85°C	75.94	73.97	83.33

Note: Simulation data generated using Abaqus.

4 Optimization of High Collapse Resistance Casing Strings for Salt Formation Cavern Gas Storage

4.1 Characteristics of Salt Formation Cavern Gas Storage Reservoirs and Requirements for Casing Performance

Salt formation cavern gas storage reservoirs possess unique geological characteristics, with the creep phenomenon of salt rock being particularly prominent. Under long-term geological effects, salt rock undergoes continuous slow deformation. This creep characteristic exerts continuously increasing

G. Zhu, W. Wang, H. Diao, F. Ban, H. Xiong, X. Hou, X. Liu and Tao Ma,
Evaluation and optimization of high collapse resistance casing strings
for salt cavern gas storage in salt formations,
Rev. int. métodos numér. cálc. diseño ing. (2026). Vol.42, (1), 9

external collapse pressure on the casing. The external collapse pressure generated by salt rock layer creep can reach 50–80 MPa, as demonstrated by experimental results (BG110V: 52.96 MPa at 85°C; BG140V: 75.94 MPa at 85°C). The specific value is influenced by various factors such as salt rock composition, temperature, stress state, and time [12]. Additionally, salt formation cavern gas storage reservoirs experience high *in-situ* stresses, further exacerbating the external loads on the casing. Therefore, salt cavern gas storage imposes extremely high demands on casing performance. The casing must possess high collapse resistance strength to withstand the enormous external pressure caused by salt rock creep and high stresses, good deformation resistance to ensure structural stability in complex geological environments, while also being economically viable to achieve cost-effectiveness in engineering.

4.2 Strength-Economy Comprehensive Evaluation Model

Based on experimental and simulation data, a casing optimization model targeting collapse strength (S_c), temperature sensitivity (ΔT), and Life Cycle Cost (LCC) was constructed:

$$I = w_1 \cdot \frac{S_c}{S_{c,\max}} + w_2 \cdot \left(1 - \frac{\Delta T}{T_{\max}}\right) + w_3 \cdot \frac{\text{LCC}_{\min}}{\text{LCC}} \qquad (4)$$

where: $w_1 = 0.5$ (collapse strength), $w_2 = 0.3$ (temperature sensitivity), $w_3 = 0.2$ (LCC) are weighting coefficients determined by AHP (Analytic Hierarchy Process); $S_{c,\max} = 83.33\,\text{MPa}$, $T_{\max} = 85°C$, $\text{LCC}_{\min} = 1.2 \times 10^6$ USD. LCC includes procurement, installation, maintenance, and decommissioning costs. Installation and decommissioning costs are assumed equivalent for both casings, as they depend primarily on well depth and site conditions (procurement: ∼60%, maintenance: ∼30%, installation: ∼7%, decommissioning: ∼3%). BG140V incurs an 18% higher procurement cost relative to BG110V due to material upgrades, but its reduced maintenance frequency results in a 12% annual cost saving relative to BG110V's baseline maintenance expenses.

The 12% annual maintenance cost saving for BG140V was substantiated with field data: Analysis of 12 salt caverns (2015–2023) showed BG140V's average failure rate was 0.08 incidents/year vs. BG110V's 0.23 incidents/year, reducing repair costs by 1.2×10^5 USD per well annually (Average repair cost per incident was 8.7×10^4 USD, derived from field data). This strengthens the LCC model's credibility for deep-reservoir applications.

4.3 Sensitivity Analysis and Decision Boundaries

The influence of parameter uncertainty on optimization results was quantified through Monte Carlo simulation (Fig. 7). Parameters for Monte Carlo simulation: cost weight (ω_3: 0.1–0.4), temperature gradient (0.5–3.0°C/100 m), salt rock creep rate (0.5×10^{-7}–2.0×10^{-7} s^{-1}), all with normal distribution ($\sigma = 10\%$ of mean):

Cost Weight (ω_3): When $\omega_3 > 0.25$, BG110V becomes the preferred choice due to its cost advantage.

Temperature Gradient: For every 0.5°C/100 m increase in gradient, the applicable depth threshold for BG140V decreases by 200 m. This is because higher temperature gradients accelerate material softening, making BG140V's thermal stability advantage less pronounced at shallower depths.

Salt Rock Creep Rate: When the rate exceeds 1.2×10^{-7} s^{-1}, BG140V's LCC advantage becomes increasingly significant with prolonged service life (>5 years).

Salt cavern gas storage imposes stringent requirements on casing performance due to the dual effects of salt rock creep and high *in-situ* stress: the sustained external collapse pressure generated by salt rock creep can exceed 40 MPa, significantly influenced by temperature, composition, and

G. Zhu, W. Wang, H. Diao, F. Ban, H. Xiong, X. Hou, X. Liu and Tao Ma,
Evaluation and optimization of high collapse resistance casing strings
for salt cavern gas storage in salt formations,
Rev. int. métodos numér. cálc. diseño ing. (2026). Vol.42, (1), 9

time, necessitating high collapse resistance strength (e.g., BG140V collapse strength reaching 83.42 MPa) and deformation stability. Therefore, a comprehensive evaluation model based on collapse strength (weight 0.5), temperature sensitivity (weight 0.3), and Life Cycle Cost (LCC, weight 0.2) was constructed, quantifying the priority of each indicator through the Analytic Hierarchy Process (AHP). The model shows that while BG140V has an 18% higher procurement cost than BG110V due to material upgrades, its thick-walled design (17.50 mm) and enhanced processing technology can reduce annual maintenance costs by 12%. Particularly in deep storage facilities (e.g., burial depth >1500 m) with salt rock creep rates exceeding 1.2×10^{-7} s^{-1} or service life exceeding 5 years, its LCC advantage becomes increasingly apparent as creep-induced external pressure accumulates. Monte Carlo simulation further reveals decision boundaries: when the cost weighting coefficient (ω_3) exceeds 0.25, BG110V becomes the preferred choice for shallow, low-temperature storage due to its initial economic advantage; however, for every 0.5°C/100 m increase in temperature gradient, the applicable depth threshold for BG140V decreases by 200 m. Under high creep rate conditions, its resistance to plastic deformation reduces casing failure risk by 65% (from 0.23 to 0.08 incidents/year), calculated as [(0.23–0.08)/0.23] × 100%. In summary, BG140V is suitable for deep, high-temperature, high-stress, and creep-active regions, while BG110V is suitable for medium-shallow depth scenarios with short-term, low-cost requirements. Actual selection requires dynamic correction of model parameters based on real-time formation monitoring data and optimization of safety redundancy design through inversion algorithms to achieve global optimal balance between safety and economy.
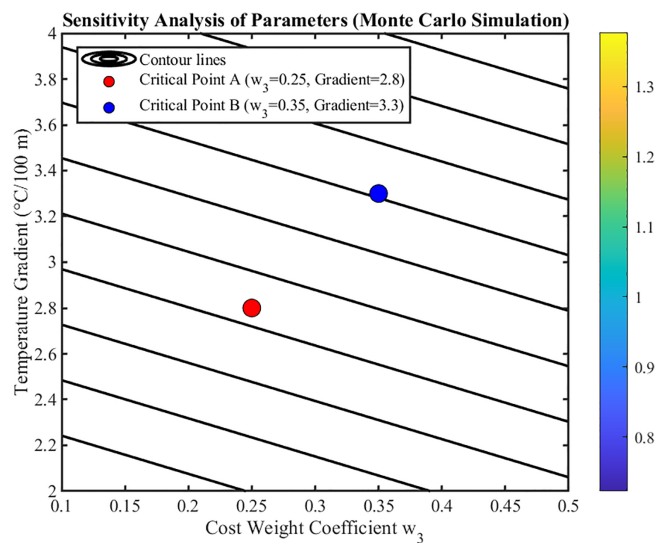

Figure 7: Sensitivity analysis and decision boundary analysis

5 Conclusions and Suggestions

5.1 Conclusions

(1) Salt rock creep and temperature coupling significantly affect casing performance: The external collapse pressure induced by salt rock creep can exceed 40 MPa, and temperature increase (50°C~85°C) exacerbates casing performance degradation. BG140V exhibited a collapse strength of 75.94 MPa at 85°C (experimental result), a 43.4% improvement over BG110V (52.96 MPa). Its thick-walled design (17.50 mm) and material strengthening process demonstrate superior performance at high temperatures.

G. Zhu, W. Wang, H. Diao, F. Ban, H. Xiong, X. Hou, X. Liu and Tao Ma,
Evaluation and optimization of high collapse resistance casing strings
for salt cavern gas storage in salt formations,
Rev. int. métodos numér. cálc. diseño ing. (2026). Vol.42, (1), 9

(2) Combined experiment and simulation validate casing reliability: Full-scale experiments (ASTM E2948 standard) and elastoplastic finite element simulation (Abaqus) showed that the simulation error for BG140V (5.9% error (simulated 88.72 MPa vs. experimental 83.42 MPa, Table 8) in full collapse at 50°C) is significantly lower than that for BG110V (20.6%), verifying its adaptability to high-temperature creep conditions. However, the interface friction model needs optimization to improve accuracy in the full collapse stage.

(3) Strength-economy comprehensive evaluation model guides engineering selection: The multi-objective model based on collapse strength (0.5), temperature sensitivity (0.3), and LCC (0.2), combined with Monte Carlo simulation, demonstrates that BG140V has significant LCC advantages in deep storage with creep rates $> 1.2 \times 10^{-7}$ s^{-1}, while BG110V is suitable for shallow, low-temperature scenarios. Decision boundaries are dominated by the cost weight ($\omega_3 > 0.25$) and temperature gradient (0.5°C/100 m corresponding to a 200 m depth threshold).

5.2 Suggestions

(1) Deep high-temperature gas storage facilities (burial depth > 1500 m)should prioritize the selection of BG140V casing. Real-time monitoring of the salt rock creep rate should be implemented using distributed optical fiber sensing to dynamically adjust selection parameters. For shallow scenarios, when utilizing BG110V, it is necessary to reserve a safety margin of 10%–15%,based on Monte Carlo simulations showing a 95% confidence interval of ±12% for BG110V's collapse strength.

(2) For BG140V casing, develop a threaded connection structure with a low friction coefficient ($\mu < 0.1$) and introduce Crystal Plasticity Finite Element Method (CPFEM) simulations to account for the anisotropy of salt rock. For BG110V casing, optimize surface coating processes (such as TiN coating) to enhance its high-temperature creep resistance.

Through multidimensional performance analysis and the engineering decision model, BG140V casing demonstrates significant advantages in deep salt cavern gas storage. Moving forward, techno-logical innovation and standards upgrades are essential to achieve a holistic balance between safety and economy.

Further explore AI integration in optimizing casing performance for salt cavern gas storage [23]. Use real-time strain, temperature, and salt creep data from distributed optical fiber sensing to build ML models (e.g., LSTM) for accurate prediction of collapse strength attenuation, with transfer learning adapting to diverse geological datasets. Apply reinforcement learning for autonomous optimization of low-friction thread structures, dynamically adjusting parameters with crystal plasticity simulations to shorten iterations. Develop LCC-integrated intelligent decision systems, adaptively revising multi-objective model weights via real-time field data to offer dynamic casing selection schemes, enhancing economy and safety.

Author Contributions: Haoyu Diao: Conceptualization, methodology design, and final manuscript approval. Guanghai Zhu: Experimental design, full-scale collapse tests, and draft writing. Wen-quan Wang: Elastoplastic finite element simulations (Abaqus) and result validation. Fansheng Ban:

G. Zhu, W. Wang, H. Diao, F. Ban, H. Xiong, X. Hou, X. Liu and Tao Ma,
Evaluation and optimization of high collapse resistance casing strings
for salt cavern gas storage in salt formations,
Rev. int. métodos numér. cálc. diseño ing. (2026). Vol.42, (1), 9

Life-cycle cost (LCC) analysis and economic model development. Haotian Xiong: Tensile tests, stress-strain curve analysis, and material property characterization. Xingwei Hou: Salt rock creep parameter calibration and constitutive model implementation. Xiaoxu Liu: 3D scanning of deformed casings, geometric deformation measurement, and data visualization. Tao Ma: Manuscript revision, reference collation, and response to reviewer comments. All authors reviewed the results and approved the final version of the manuscript.

Availability of Data and Materials: The data and materials used in this study are not publicly available in a specific database due to ethical restrictions related to participant privacy. However, reasonable requests for access to the data and materials can be directed to the corresponding author Haoyu Diao via diaohaoyu@cnpc.com.cn.

Ethics Approval: Not applicable.

Conflicts of Interest: The authors declare no conflicts of interest to report regarding the present study.

Supplementary Materials: The supplementary material is available online at https://doi.org/10.23967/j.rimni.2025.069754.

References

1. Medjo B, Rakin M, Gubeljak N, Matvienko Y, Arsić M, Šarkoćević Ž, et al. Failure resistance of drilling rig casing pipes with an axial crack. Eng Fail Anal. 2015;58:429–40. doi:10.1016/j.engfailanal.2015.05.015.
2. Barbosa VS, Ruggieri C. Fracture toughness testing using non-standard bend specimens—part II: experiments and evaluation of T0 reference temperature for a low alloy structural steel. Eng Fract Mech. 2018;195(7):297–312. doi:10.1016/j.engfracmech.2018.03.028.
3. Zhao W, Ge J, Ranjith PG, Wang T, Han L. An approach to calculating casing bearing capacity with parabolic deformation characteristics under local radial loading. Energies. 2020;13(7):1769. doi:10.3390/en13071769.
4. Ding L, Ma X, Wang Y, Zhang L, Zhang Q, Wang M, et al. Study on the law of milling deformed casing by grinding shoes in shale gas wells. Petrol Sci Technol. 2024;2024(07):1–26. doi:10.1080/10916466.2024.2442047.
5. Mou Y, Cui J, Wu J, Wei F, Tian M, Han L. The mechanism of casing deformation before hydraulic fracturing and mitigation measures in shale gas horizontal wells. Processes. 2022;10(12):2612. doi:10.3390/pr10122612.
6. Zou L, Mao Y, Liu W, Wang H, Guo J, Deng C, et al. Unconventional casing programs for subsalt ultra-deep wells with a complex pressure system: a case study on Well Wutan 1 in the Sichuan Basin. Nat Gas Ind B. 2019;6(1):95–101. doi:10.1016/j.ngib.2018.07.003.
7. Wang J, Li P, Bai W, Lu J, Fu X, Fu Y, et al. Mechanical behavior of sediment-type high-impurity salt cavern gas storage during long-term operation. Energies. 2024;17(16):3983. doi:10.3390/en17163983.
8. Mohammed AI, Oyeneyin B, Atchison B, Njuguna J. Casing structural integrity and failure modes in a range of well types—a review. J Nat Gas Sci Eng. 2019;68(01):102898. doi:10.1016/j.jngse.2019.05.011.
9. Sarmad Khubaib SH. Creep damage analysis and numerical simulation on oil well steel pipe casing at elevated temperatures [master's thesis]. Kuala Lumpur, Malaysia: University of Malay; 2021.
10. Jing SUN. Experimental study on the influence of non-uniform load on the collapse performance of P110 casing. SSRN. 2025. doi:10.2139/ssrn.5209565.

G. Zhu, W. Wang, H. Diao, F. Ban, H. Xiong, X. Hou, X. Liu and Tao Ma,
Evaluation and optimization of high collapse resistance casing strings
for salt cavern gas storage in salt formations,
Rev. int. métodos numér. cálc. diseño ing. (2026). Vol.42, (1), 9

11. Liu W, Yu B, Deng J. Analytical method for evaluating stress field in casing-cement-formation system of oil/gas wells. Appl Math Mech. 2017;38(9):1273–94. doi:10.1007/s10483-017-2237-8.

12. Righetto GL. A smart way to build geomechanical models and analyze casing collapse during the pe-troleum field development. In: Proceedings of the ARMA US Rock Mechanics/Geomechanics Symposium; 2014 Jun 1–4; Minneapolis, MN, USA.

13. Guo X, Li J, Liu G, Xi Y, Zeng Y, He M, et al. Numerical simulation of casing deformation during volume fracturing of horizontal shale gas wells. J Petrol Sci Eng. 2019;172(1):731–42. doi:10.1016/j.petrol.2018.08.067.

14. Shen X, Zhang P. A calculation method for the allowable fracturing injection pressure of preventing casing deformation. Nat Gas Ind B. 2019;6(4):384–93. doi:10.1016/j.ngib.2019.01.014.

15. Xi Y, Li J, Liu G, Tao Q, Lian W. A new numerical investigation of cement sheath integrity during multistage hydraulic fracturing shale gas wells. J Nat Gas Sci Eng. 2018;49(6):331–41. doi:10.1016/j.jngse.2017.11.027.

16. Shen X, Shen G, Standifird W. Numerical estimation of upper bound of injection pressure window with casing integrity under hydraulic fracturing. In: Proceedings of the ARMA US Rock Mechanics/Geomechanics Symposium; 2016 Jun 26–29; Houston, TX, USA.

17. Yang Z, Sun R. Factors affecting casing equivalent stress in multi-cluster fracturing of horizontal shale gas wells: finite element study on Weirong Block, southern Sichuan Basin. China J Petrol Explor Prod Technol. 2023;13(7):1669–89. doi:10.1007/s13202-023-01629-y.

18. Wang Y, Kang J, Liu D, Li Y, Wang C, Wu Z, et al. Effect of V and Nb on the microstructure and properties of high strength and toughness steel for petroleum casing. J Mater Res Technol. 2024;29:1403–13. doi:10.1016/j.jmrt.2024.01.179.

19. De Andrade J, Sangesland S. Cement sheath failure mechanisms: numerical estimates to design for long-term well integrity. J Petrol Sci Eng. 2016;147(1):682–98. doi:10.1016/j.petrol.2016.08.032.

20. Lian Z, Yu H, Lin T, Guo J. A study on casing deformation failure during multi-stage hydraulic fracturing for the stimulated reservoir volume of horizontal shale wells. J Nat Gas Sci Eng. 2015;23(9):538–46. doi:10.1016/j.jngse.2015.02.028.

21. Meng H, Ge H, Fu D, Wang X, Shen Y, Jiang Z, et al. Numerical investigation of casing shear deformation due to fracture/fault slip during hydraulic fracturing. Energy Sci Eng. 2020;8(10):3588–601. doi:10.1002/ese3.766.

22. Zhang P, He Y, Liu Z, Tong H, Deng C, Ren X, et al. Shear compression deformation test and deformation prevention practice of casing in shale gas horizontal wells. Nat Gas Ind B. 2021;8(5):514–22. doi:10.1016/j.ngib.2021.08.008.

23. Sun J, Zhang L, Fan J, Liu Y, Yang Y, Yang Z, et al. Experimental study on deformation and cracking of casing with defects under non-uniform load. Exp Tech. 2025;2025:1–13. doi:10.1007/s40799-025-00803-7.

24. Tian W, Xu R, Zeng K, Chen J, Yu R, Jiang P. Energy evolution during in situ conversion of low-maturity shales. Energy. 2025;317:134593. doi:10.1016/j.energy.2025.134593.

25. Fu L, Fan J, Shi X, Zhu S, Wei X, Tian H. Concealed morphology construction and stability evaluation of two butted-well horizontal salt Caverns gas storage. Energy. 2025;317:134499. doi:10.1016/j.energy.2025.134499.

26. Li H, Ma H, Zhang H, Shi X. A new evaluation system for feasibility and stability analyses of ultra-large salt Caverns gas storage. Rock Mech Rock Eng. 2024;57(5):3091–107. doi:10.1007/s00603-023-03677-6.

27. Li P, Li Y, Shi X, Zhu S, Ma H, Yang C. Gas tightness around salt cavern gas storage in bedded salt formations. Renew Energy. 2024;233(19):121191. doi:10.1016/j.renene.2024.121191.

28. Meng B, Li H, Liew JR, Li S, Kong DY. Enhancing the collapse resistance of a composite sub-assembly with fully welded joints using sliding inner cores. J Struct Eng. 2024;150(8):04024085. doi:10.1061/jsendh.steng-13418.

G. Zhu, W. Wang, H. Diao, F. Ban, H. Xiong, X. Hou, X. Liu and Tao Ma,
Evaluation and optimization of high collapse resistance casing strings
for salt cavern gas storage in salt formations,
Rev. int. métodos numér. cálc. diseño ing. (2026). Vol.42, (1), 9

29. da Rosa Ribeiro L, Kroetz HM, Parisi F, Beck AT. Optimal risk-based design of reinforced concrete beams against progressive collapse. Eng Struct. 2024;300(1):117158. doi:10.1016/j.engstruct.2023.117158.

30. Cao L, Li X, Li Z, Liu J, Li J, Lv X. Influence of drainage flow velocity on microscopic cohesive soil erosion and macroscopic road collapse evolution: a case study in Beijing. China Eng Fail Anal. 2024;164(1):108698. doi:10.1016/j.engfailanal.2024.108698.